Progress In Electromagnetics Research, PIER 13, 243–291, 1996

A NEW EQUIVALENT NETWORK APPROACH TO ELECTROMAGNETIC WAVE PROBLEMS

H. Shigesawa and M. Tsuji

1. Introduction

The general electromagnetic fields can be represented by the superposition of plane waves traveling in diverse directions [l]. Once this idea is employed in radiation, diffraction and guided-wave problems, the electromagnetic fields are expressed by the Fourier integral in which the behavior of plane waves traveling in diverse directions is represented in terms of a spectral continuum of wavenumber defined on any

plane transverse to a coordinate axis, e.g., the z axis. Such a plane-wave spectral representation of solutions of Maxwell's equations is simple in its mathematical formulation, and its use is certainly straightforward to explain some of important electromagnetic-field problems to be constructed by the elaborate type of solutions.

In an unbounded homogeneous space, for example, the plane-wave spectrum of fields is essentially continuous, while, in a bound space like cavity resonators or waveguides of closed type, the plane-wave spectrum becomes discrete. On the other hand, in the problems of wave propagation over homogeneous plane surfaces, e.g., impedance planes, dielectric layers and so on, the plane-wave spectrum is generally split into two parts: one is the continuous part and the other is the discrete one, and the total field can be regarded as a superposition of these different types of the constituent spectrum. The waves with continuous and discrete spectra are often called as "radiation" or "space wave" and "surface wave", respectively. If such homogeneous plane surfaces are appropriately deformed, some parts of the plane-wave spectrum often construct another type of discrete-spectral wave what we call "leaky wave."

For a range of electromagnetic-wave problems, solutions are indeed obtained formally with mathematical completeness straightforwardly by means of the plane-wave spectral representation, but the numerical approach using the fields constructed by such solutions is not always effective to solve somewhat complicated problems of the electromagnetic field. Some of typical examples will be discussed in this chapter.

As an example, let us consider the nature of waves on an unbounded dielectric slab which occupies the region between $y = t$ and $-t$ (see Fig. 1). We assume here that the properties of the structure are independent of x and z, and the half space extending above or below the slab is homogeneous free space. Then in general the reflection coefficient looking into the negative y direction at $y = t$ will have poles which are related to surfacewave modes. Then the residual term of the integration is expressed by the branch-cut integral that relates to the contribution of radiation waves. Thus we must always consider both radiation wave and surface-wave modes simultaneously; they are, however, quite different to each other, in nature, at least in the mathematical sense, because the radiation wave is not characterized by a unique propagation constant along the z axis like a surface-wave mode

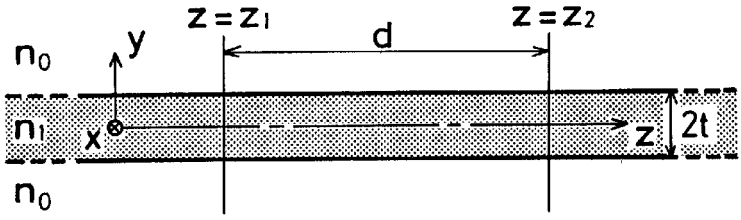

Figure 1. Planar dielectric waveguide uniform in the x direction.

is singular in the sense that the radiation wave with different transverse wave-numbers are governed orthonormally by the Dirac delta function. Then the power carried by the radiation wave is known only if a spectral representation of fields is doubly integrated in both spectral and space domains. This point is particularly different from the nature of surface-wave modes; their orthogonality is presented by the Kronecker delta symbol, so that the power carried by each surface-wave mode is known by integrating the modal distribution in space domain alone. Such a difference in mathematical nature between radiation waves and surface-wave modes has been a main reason which makes it almost impossible to develop a simple and effective equivalent network approach for analyzing the problems of unbounded dielectric slabs mentioned above, although an equivalent network approach is quite familiar to the microwave engineers as faced in closed-waveguide problems [2–3].

This chapter describes a breakthrough to such a difficulty [4–6]. Our idea recomposes the radiation waves into a discrete set of an infinite number of newly defined so called "spectral composite" modes [7]. These new modes, in conjunction with surface-wave modes, construct a complete-orthonormal set for expressing an arbitrary local field on any plane transverse to the z axis. It is then proved that each of spectral composite modes carries a finite magnitude of radiation power according to the orthonormal relation expressed not by the Dirac delta function, but by the Kronecker delta symbol like the surface-wave modes. As a result, we can provide the modal voltages and currents for the spectral composite modes in identical fashion with those for the surface-wave modes. This means that we can picture a simple network model allocated the discrete terminal ports to each of both types of modes, and that we can use the modal voltages and currents mentioned above to define the terminal parameters (e.g., the

root power amplitude, the wave impedance and so on) at each terminal port. In the following section, we will discuss the equivalent network representation for several types of the typical structures.

2. General Approach

2.1 Spectral Composite Modes and Equivalent Network Representation for a Homogeneous Dielectric Waveguide.

We first consider a homogeneous dielectric slab waveguide as shown in Fig. l, which is symmetric with respect to the xz plane at $y = 0$. We assume here that the fields are polarized in the x direction and the waveguide can support M surface-wave modes. Applying the boundary conditions at $y = t$, we can express the total fields in terms of the orthonormal modal functions of both surface-wave modes and the radiation "modes" [4], instead of the plane-wave spectral representation. Let $e_{xj}(y)$, $h_{yj}(y)$ and $e_x(y,\rho)$, $h_y(y,\rho)$ be the orthonormal modal functions of the jth surface-wave mode and the radiation modes, respectively (see [8] for the functional forms). Here, ρ denotes the transverse wavenumber of the radiation mode along the y axis outside the slab. Each type of modal functions is normalized in terms of the Kronecker delta symbol or the Dirac delta function as noted in [8, sec.8.5]. Although the wavenumber ρ covers all the values from 0 to ∞, the radiation modes in the range $0 < \rho < n_0 k_0$ are propagating to the z direction, while those in the range $n_0 k_0 < \rho < \infty$ are non-propagating. Therefore, the total electric field $E_x(y, z_1)$ on the plane at $z = z_1$ is completely expressed by the following equation [5]:

$$E_x(y,z_1) = \sum_{m=0}^{M-1} A_m(z_1) e_{xm}(y) + \int_0^{n_0 k_0} f(\rho, z_1) e_x(y,\rho) d\rho + \int_{n_0 k_0}^{\alpha n_0 k_0} g(\rho, z_1) e_x(y,\rho) d\rho \tag{1}$$

where $f(\rho, z_1)$ and $g(\rho, z_1)$ are the continuous spectral functions for the radiation modes at $z = z_1$ and the coefficients $A_m(z_1)$ stand for the root-power amplitudes of the surfacewave modes. Now, the electric field of (1) after traveling up to the plane at $z = z_2$ toward the positive

z direction ($z_2 > z_1$ with $d = z_2 - z_1$) can be written as follows;

$$E_x(y, z_2) = \sum_{m=0}^{M-1} B_m(z_2) e_{xm}(y) + \int_0^{n_0 k_0} f(\rho, z_2) e_x(y, \rho) d\rho + \int_{n_0 k_0}^{\alpha n_0 k_0} g(\rho, z_2) e_x(y, \rho) d\rho \tag{2}$$

where

$$\begin{aligned} B_m(z_2) &= A_m(z_1) e^{-j\beta_m d} \\ f(\rho, z_2) &= f(\rho, z_1) e^{-j\beta(\rho) d} \\ g(\rho, z_2) &= g(\rho, z_1) e^{-\gamma(\rho) d} \end{aligned} \tag{3}$$

β_m is the phase constant of the m th surface-wave mode, while $\beta(\rho) = \sqrt{(n_0 k_0)^2 - \rho^2}$ and $\beta(\rho) = -j\sqrt{\rho^2 - (n_0 k_0)^2} = -j\gamma(\rho)$ are the phase constants of the propagating and the nonpropagating radiation modes, respectively. The modal functions of both surface-wave modes and radiation modes in (1) and (2) do not change as they propagate along the guide axis, but their complex amplitude and the continuous spectral amplitude change. The change in the complex amplitude of each surface-wave mode is easily pictured by the simple network model consisting of uncoupled parallel transmission lines. Then, there is a one-to-one correspondence between $A_m(z_1)$ and $B_m(z_2)$ for each surface-wave mode. While the constitutive component of $E_x(y, z_2)$ corresponding to the radiation mode shown by the branch-cut integral in (2), varies in its resultant functional form along the y axis as the radiation mode propagates the distance d, although the amplitude of the spectral functions $f(\rho, z_2)$ and $g(\rho, z_2)$ are simply related to $f(\rho, z_1)$ and $g(\rho, z_1)$, respectively, through (3). Our motivation here is to express such a varying field by a similar expansion form with the surface-wave field as seen in the first term of the right hand side of (2). To this end, recalling $e_x(y, \rho)$ to be independent of z, it is quite natural to expand $f(\rho, z_1)$ and $g(\rho, z_1)$ into a complete set of the orthonormal functions $\phi_n(\rho)$ and $\psi_n(\rho)$ of only ρ as follows:

$$\begin{aligned} f(\rho, z_1) &= \sum_{n=0}^{N-1} A_{M+n}(z_1) \phi_n(\rho) \\ g(\rho, z_1) &= \sum_{n=0}^{N-1} A_{M+N+n}(z_1) \psi_n(\rho) \end{aligned} \tag{4}$$

where

$$\int_0^{n_0k_0} \phi_m(\rho)\phi_n(\rho)d\rho = \delta_{mn}$$
$$\int_{n_0k_0}^{\alpha n_0k_0} \psi_m(\rho)\psi_n(\rho)d\rho = \delta_{mn} \tag{5}$$

Similar expansions hold for the spectral functions $f(\rho, z_2)$ and $g(\rho, z_2)$ by replacing $A_{M+n}(z_1)$ and $A_{M+N+n}(z_1)$ in (4) with $B_{M+n}(\rho, z_2)$ and $B_{M+N+n}(\rho, z_2)$, respectively. A reasonable choice for the set of expansion functions used in (4) will be explained in the next section. Here, it should be noted that the expansion coefficients $A_i(z)$ and $B_i(z)$ are still functions of z because the continuous spectral functions are deformed as the radiation modes propagate along the guide. Then we modify further the expansions of (4) to obtain a discrete set of an infinite number of what are called spectral composite modes, defined by

$$\tilde{e}_{xn}(y) = \int_0^{n_0k_0} \phi_n(\rho)e_x(y, \rho)d\rho$$
$$\hat{e}_{xn}(y) = \int_{n_0k_0}^{\alpha n_0k_0} \psi_n(\rho)e_x(y, \rho)d\rho \tag{6}$$

It is easily proven that these spectral composite modes have orthonormal relations subject not to the Dirac delta function but to the Kronecker delta symbol (see Appendix I). Substituting (4) into (3) and applying the definition (6), (1) and (2) can be reduced to the forms

$$E_x(y, z_1) = \sum_{m=0}^{M-1} A_m(z_1)e_{xm}(y) + \sum_{n=0}^{N-1} [A_{M+n}(z_1)\tilde{e}_{xn}(y) + A_{M+N+n}(z_1)\hat{e}_{xn}(y)] \tag{7}$$

$$E_x(y, z_2) = \sum_{m=0}^{M-1} B_m(z_2)e_{xm}(y) + \sum_{n=0}^{N-1} [B_{M+n}(z_2)\tilde{e}_{xn}(y) + B_{M+N+n}(z_2)\hat{e}_{xn}(y)] \tag{8}$$

Since the modal functions of all modes in (7) and (8) are now subject to the orthonormal relation expressed by the Kronecker delta symbol, we can picture a simple terminal model for the equivalent

network of a homogeneous dielectric waveguide at least at the local position at $z = z_1$ or z_2; one of the terminal ports can be allocated to each of spectral composite modes and surface-wave modes. However, the amplitude, for example, $A_{M+n}(z_1)$ of the spectral composite mode changes in its magnitude as well as in its phase as it propagates. Such a difference in the magnitudes between two positions at $z = z_1$ and z_2 reminds us that there is no longer any one-to-one correspondence between A_{M+n} and B_{M+n} or A_{M+N+n} and B_{M+N+n}, and one of the input spectral-composite modes at $z = z_1$ necessarily couples to all of the output spectral composite modes at $z = z_2$ while it propagates. Let us then substitute $f(\rho, z_1)$ of (4) into that of (3) to obtain

$$\sum_{n=0}^{N-1} B_{M+n}(z_2)\phi_n(\rho) = \sum_{k=0}^{N-1} A_{M+k}(z_1)\phi_k(\rho)e^{-j\beta(\rho)d}d\rho \tag{9}$$

where the coefficients $A_q(z_i)$ and $B_q(z_i)$ are defined so as to stand for the root-power amplitude of the spectral composite mode. By using the orthonormal relation of $\phi_n(\rho)$, we have

$$B_{M+n}(z_2) = \sum_{k=0}^{N-1} \tilde{S}_{nk} A_{M+k}(z_1) \tag{10}$$

where

$$\tilde{S}_{nk} = \int_0^{n_0 k_0} \phi_n(\rho)\phi_k(\rho)e^{-j\beta(\rho)d}d\rho \tag{11}$$

By following the same procedure, we have

$$B_{M+N+n}(z_2) = \sum_{k=0}^{N-1} \hat{S}_{nk} A_{M+N+k}(z_1) \tag{12}$$

where

$$\hat{S}_{nk} = \int_{n_0 k_0}^{\alpha n_0 k_0} \psi_n(\rho)\psi_k(\rho)e^{-\gamma(\rho)d}d\rho \tag{13}$$

If any field distribution given at $z = z_2$ propagates to the negative z direction, the resultant field at $z = z_1$ can be expressed by relations similar to (10) and (12). As a result, the equivalent network for a homogeneous dielectric waveguide of length d, sandwiched with two infinite xy planes at $z = z_1$ and $z = z_2$, can be represented by Fig. 2

and the terminal amplitudes are governed by the matrix $[S_{LINE}]$ given in Appendix II. The formulation presented here, although seen to be familiar on the surface, is new in the sense that it makes it possible to analyze the problem of interacting discontinuities on open structures by the network approach that is well developed in problems of closed waveguides.

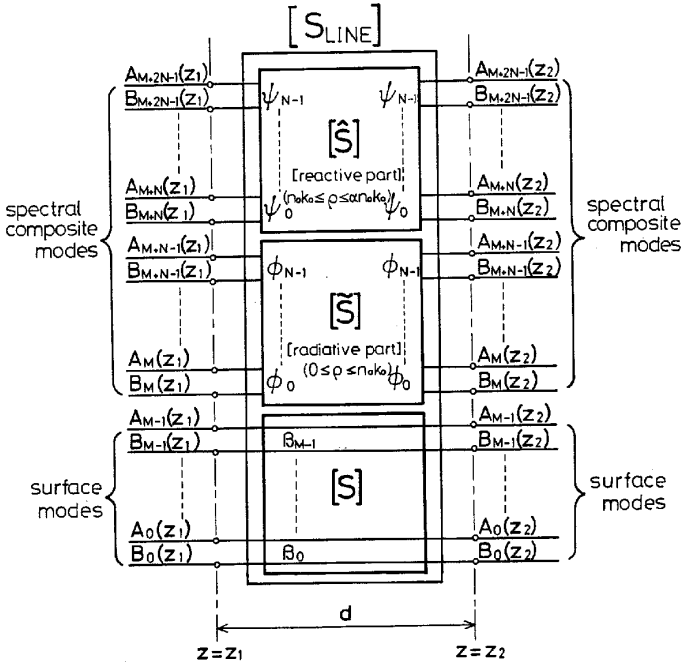

Figure 2. Equivalent network representation $[S_{LINE}]$ for the homogeneous slab waveguide, where the spectral composite modes are newly introduced by using the complete orthonormal functions ϕ_n and ψ_n defined in each range of ρ indicated in the networks $[\tilde{S}]$ and $[\hat{S}]$, respectively.

2.2 Equivalent Network Representation for Free Space and Bound Half Space.

The results obtained in Sec.2.1 are effectively used to derive an equivalent network representation of homogeneous free space or half space bounded by short-circuit plane or open-circuit plane. Let us first consider the free space. It is obvious that the free space is simply

realized by removing the dielectric slab in Fig. 1. Therefore an x-polarized electric field $E_x(y,z)$, for example, is represented only by the branch-cut integrals appeared in (1) and (2), by dropping the surface-wave term (the first term of the right hand side). For the free-space case, the modal function $e_x(y,\rho)$ of the radiation modes is, of course, given by a combination of sine and cosine functions along the entire y axis. This replacement must be done for all of the equations appeared in Sec.2.1. As a result, the equivalent network for a zonal free space, sandwiched with two infinite xy planes at $z = z_1$ and $z = z_2$, is expressed in terms of only the spectral composite modes by taking away the equivalent transmission lines for the surface-wave modes in Fig. 2. Such an equivalent network is denoted by the matrix $[S^f_{ZONE}]$.

Next, let us consider a half space occupying the region $y > 0$, which is realized by bisecting the full space with a short-circuit plane placed on the xz plane at $y = 0$. Then all the discussions on the equivalent network representation for the full space mentioned above can be still effectively applied to the present case, only if the sine function is employed for expressing the modal function $e_x(y,\rho)$ of the radiation modes along the entire positive y axis. On the other hand, if the half space is realized by an open circuit plane instead of a short-circuit plane, the equivalent network is represented by the one for the half space just mentioned above, if the cosine function is used for expressing the modal function $e_x(y,\rho)$.

By noting such differences in the forms of the modal function, the equivalent network denoted by the matrix $[S^h_{ZONE}]$ is easily obtained for the zonal half space.

2.3 Equivalent Network Representation for Junction Discontinuities.

In parts 2.1 and 2.2 in this section, we have discussed the structures that are uniform along the propagation axis, and derived their equivalent network matrices $[S_{LINE}]$ and $[S_{ZONE}]$ which express uniform sections of length d, sandwiched with two infinite xz planes at $z = z_1$ and z_2. Practical structures, however, do not consist of only such uniform sections, but are usually constructed by the cascade connection of different kinds of uniform sections. Then it is necessary to derive junction matrices that express the wave behavior at various types of junction plane between different two kinds of structure. Typical junction discontinuities will be those between different uni-

form waveguides, a uniform waveguide and a full space (or a dielectric-waveguide open end), and a half space and a full space (or a half-space open end). In this section, the first two junction discontinuities will be discussed. The last one often appears in electromagnetic-wave scattering and diffraction problems, so it will be discussed in Sec. 4.

Let us first derive the equivalent network for a step discontinuity between two semi-infinite homogeneous dielectric waveguides I and II with different thicknesses as shown in Fig. 3.

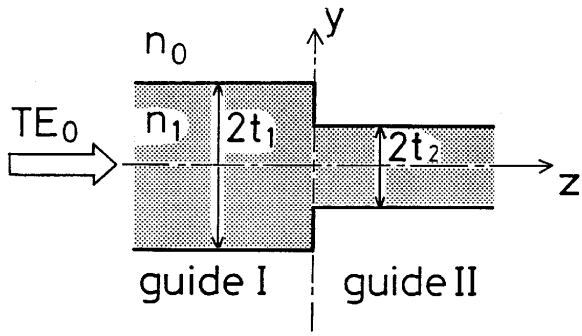

Figure 3. Step discontinuity configuration between two planar dielectric wave-guides with different thicknesses.

We consider here that one of modes is incident normally to the step from the left-hand side or the right-hand side of Fig. 3. An example of such excitations is the incidence of the qth surface-wave mode from the left-hand side. Then, the electric fields tangential to the discontinuity plane at $z = 0$ can be expressed as follows [5]:

$$E_x^I(y, 0^-) = \sum_{p=0}^{M+2N-1} (\delta_{qp} + R_{qp}) e_{xp}^I(y) \tag{14}$$

$$E_x^{II}(y, 0^+) = \sum_{p=0}^{M+2N-1} T_{qp} e_{xp}^{II}(y) \tag{15}$$

where

$$\begin{aligned} e^i_{xp}(y) &= e^i_{xm}(y) \quad \text{for } p = 0, 1, ..., M-1 \quad (m = p) \\ &= \tilde{e}^i_{xn}(y) \quad \text{for } p = M, ..., M+N-1 \quad (n = p - M) \\ &= \hat{e}^i_{xn}(y) \quad \text{for } p = M+N, ..., M+2N-1 \quad (n = p - M - N) \end{aligned} \tag{16}$$

for i = I or II.

R_{qp} and T_{qp} are the unknown coefficients to be determined. We use here the mode matching method to fit the boundary condition on the plane $z = 0$ in the sense of least mean squares [5,9], which considers the error ϵ given by the following equation:

$$\epsilon = \frac{1}{2}\left(\frac{\int_{-\infty}^{\infty} |E^I_x - E^{II}_x|^2 dy}{\int_{-\infty}^{\infty} |e^I_{xq}|^2 dy} + \frac{\int_{-\infty}^{\infty} |H^I_y - H^{II}_y|^2 dy}{\int_{-\infty}^{\infty} |h^I_{yq}|^2 dy} \right) \tag{17}$$

where H^I_y and H^{II}_y are the magnetic fields associated with the electric fields of (14) and (15), respectively, and e^I_{xq} and h^I_{yq} are the electric and magnetic fields of the incident mode.

Minimizing ϵ with respect to the unknowns by the procedures described in [5,6,9], we can easily obtain them. Applying the same procedure to all the other excitation cases, one can obtain all of the unknown coefficients R_{qp} and T_{qp} which are linked with the elements of the matrix $[S_{STEP}]$ representing the isolated step discontinuity, as mentioned in Appendix III. As a result, a step discontinuity can be expressed by the equivalent network shown in Fig. 4, which again has the terminal ports corresponding to each of the surface-wave modes and spectral composite modes. By following the same procedures, we can derive one more matrix $[S'_{STEP}]$, for the step discontinuity, whose structure is the mirror inversion of Fig. 3 with respect to the xy plane at $z = 0$.

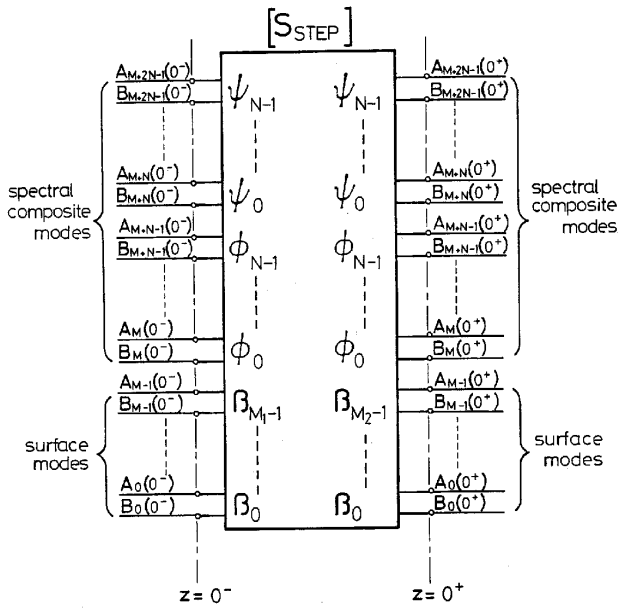

Figure 4. Equivalent network representation $[S_{STEP}]$ for the step discontinuity shown in Figure 3.

Here it is necessary to comment on a reasonable choice for a set of expansion functions in (4). The spectral composite modes of our definition are based on the expansion of the continuous spectral function partitioned into two finite ranges on the wavenumber (ρ) plane, and they are applied to the mode-matching method in the form of (17). This problem is mathematically the best approximation calculation based on the unweighted L^2 norm in the finite range of variables, so that the Legendre polynomials are the best basis functions [l0-11]. Therefore, we will use them throughout this chapter. Next, let us derive the equivalent network for a dielectric-waveguide open end that is a junction discontinuity between a semi-infinite homogeneous dielectric waveguide and a full space as shown in Fig. 5.

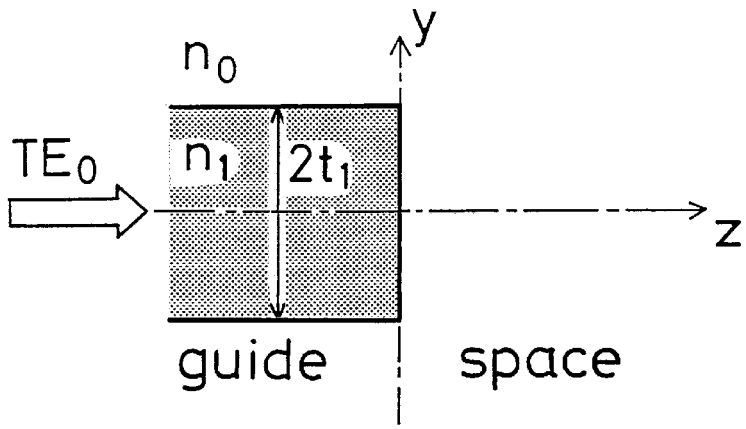

Figure 5. Discontinuity configuration of a dielectric-waveguide open end which is a junction discontinuity between a semi-infinite homogeneous dielectric waveguide and a full space.

The equivalent network for such a junction is easily derived by following the same manner with that followed in deriving the matrix $[S_{STEP}]$ or $[S'_{STEP}]$. However, the present discontinuity is realized by taking away the semiinfinite dielectric waveguide II appearing in Fig. 3 and by replacing it with a space extending semi-infinitely in the z direction. Therefore, the present equivalent network has the terminal ports corresponding to each of both surface-wave modes and spectral composite modes on its left-hand side (or the dielectric waveguide side), while the terminal ports on its right-hand side (or the space side) consist only of the spectral composite modes as shown in Fig. 6. Such a network is denoted hereafter by the matrix $[S^d_D]$.

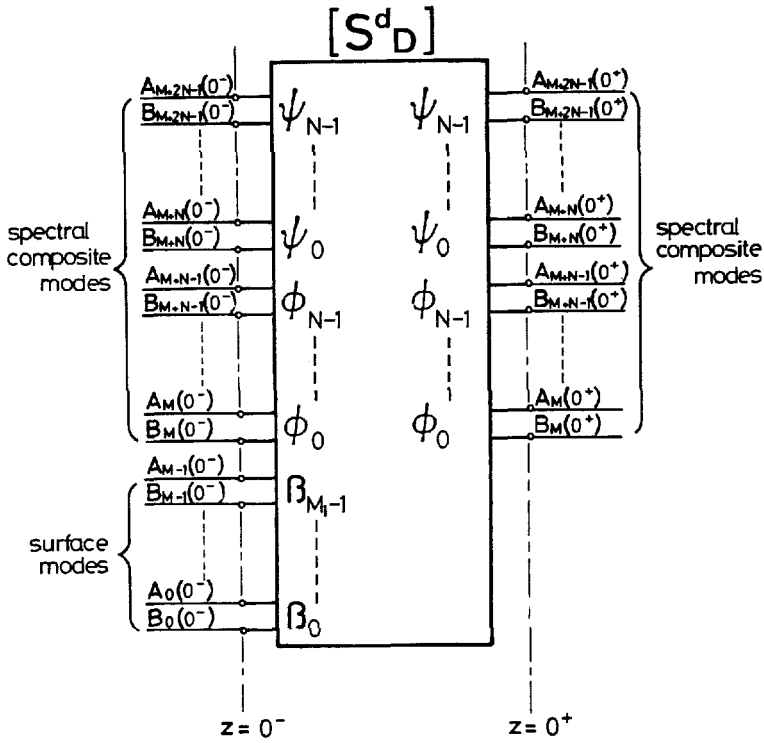

Figure 6. Equivalent network representation for a dielectric-wave guide open end shown in Figure 5.

One of remaining step discontinuities associated with $[S_D^d]$ is its mere inversion with respect to the junction plane. We denote its matrix by $[S'^d_D]$ which is easily derived by following the same procedures mentioned above.

3. Discontinuous Waveguide Structures

3.1 Mode Propagation through Symmetric Double Step.

This section discusses some practical examples: the symmetric double step shown in Figs. 7(a) and 8(a). These structures play an important role in practical planar circuits. For example, Fig. 7(a) appears as a constitutive block of dielectric grating filters[l2], while Fig. 8(a) often appears as a coupling section of planar dielectric resonators [l3].

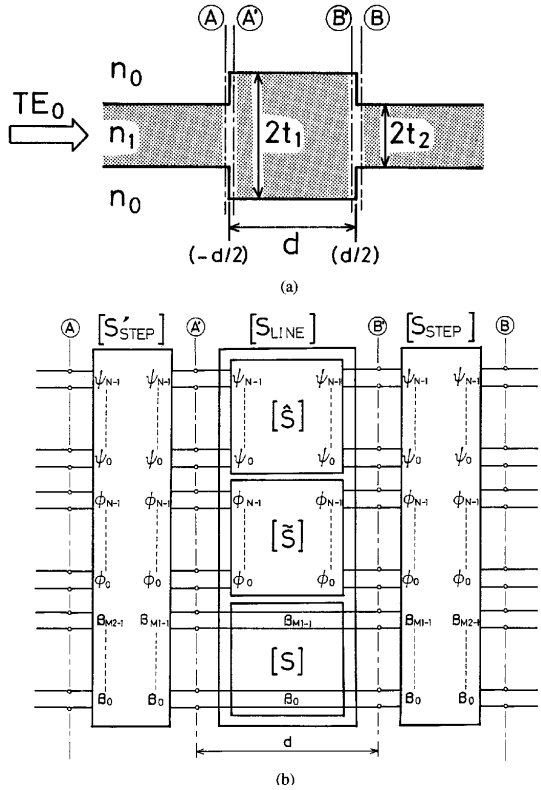

Figure 7. Symmetric double-step discontinuity: (a) The configuration on the longitudinal section and (b) Its equivalent network. The networks $[\tilde{S}]$ and $[\hat{S}]$ represent the coupling effect among the spectral composite modes in each range of ρ.

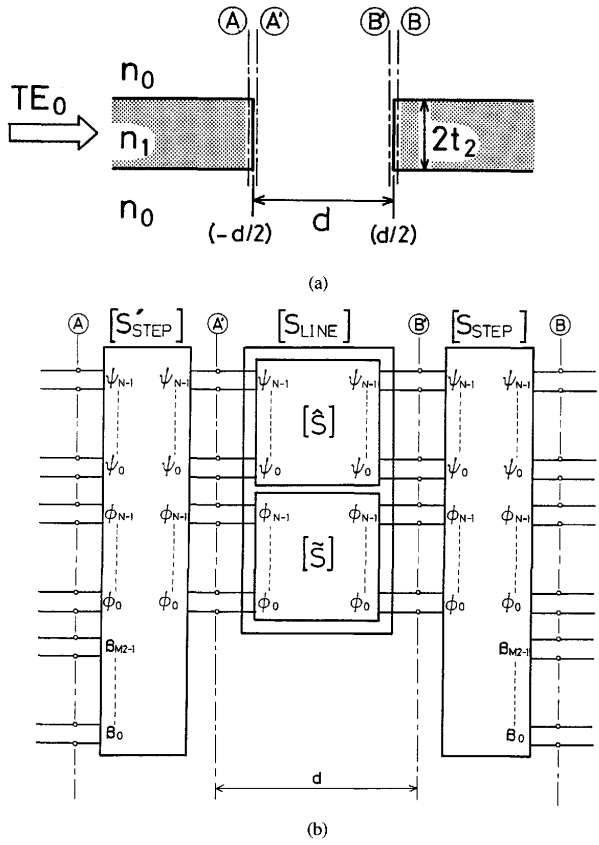

Figure 8. Symmetric double-step discontinuity with an air gap between two planar dielectric waveguides: (a) The configuration on the longitudinal section and (b) Its equivalent network.

We assume that the guide with a thickness $2t_1$ in the case of Fig. 7(a) supports M_1 surface-wave modes, while the guide with thickness $2t_2$ in the cases of both Fig. 7(a) and Fig. 8(a) supports M_2 surface-wave modes. The structure of Fig. 7(a) is partitioned into three building blocks by correctly defining the terminal planes as shown. It consists of two step discontinuities and one homogeneous waveguide of length d interconnecting the two interacting steps. By following the matrix notation for structures mentioned in Sec. 2, those building blocks can be expressed by the equivalent matrices $[S_{STEP}]$, $[S_{LINE}]$ and $[S'_{STEP}]$,

respectively. Thus, by properly connecting these matrices in tandem, the overall equivalent network is obtained as shown in Fig. 7(b). This network shows an example when only the TE_0 fundamental surface-wave mode is incident from the lefthand side of the structure (as shown), where all of the terminal ports, except for the input port of the incident surface-wave mode on the plane Ⓐ, are terminated properly by the corresponding characteristic impedance of the equivalent transmission lines for each surface-wave mode or by the matched termination impedance for each spectral composite mode (see Appendix IV). Of course, we can consider any excitation state in the similar way. On the other hand, the double step of Fig. 8(a) is an air gap between the terminal planes Ⓐ and Ⓑ so the equivalent network for this gap is expressed by $[S_{ZONE}]$, corresponding to a zonal full space, in which only the spectral composite modes can exist. Thus, we have Fig. 8(b) as the overall equivalent network for Fig. 8(a).

Now, assuming the incident TE_0 surface-wave mode with unit root-power amplitude in both Figs. 7(b) and 8(b), one can straightforwardly obtain $B_{N_1+n}(-d/2)$ and $B_{N_1+n}(d/2)$ for the nth spectral composite mode at planes Ⓐ and Ⓑ respectively, as well as $B_m(-d/2)$ and $B_m(d/2)$ of the reflected and transmitted surface-wave modes, respectively. These amplitudes give the total electric field at planes Ⓐ and Ⓑ through (7) and (8). Thus, by reconstructing the radiation fields on the terminal planes from these known amplitudes and applying the SDP approximation to the first term in the bracket of (7) and (8) expressing the spectral composite modes of the radiative part, we can calculate the fields radiated in both the forward $(+z)$ and backward $(-z)$ directions.

Numerical examples are obtained for the double step with the dimension indicated in the insets of Figs. 9 and 10. For the given values of the parameters, only the TE_0 fundamental surface-wave mode can propagate in the dielectric waveguide with thickness $2t_2$, while the waveguide of thickness $2t_1$ in Fig. 9 supports the TE_0 and TE_2 modes. The reflection coefficient R_0 and the transmission coefficient T_0 of the surface-wave mode are shown in Figs. 9(a) and 10(a), while the backward and forward radiation powers are shown in (b), as a function of the relative length d/t_2. The results indicated by the solid curves are calculated by using a scale factor of $\alpha = 7$ and by taking the expansion terms of the Legendre function as $N = 9$ (satisfactory convergence of solutions has been confirmed in [4]). The results for

only R_0 and T_0 can be compared with those in the published papers [14-16].

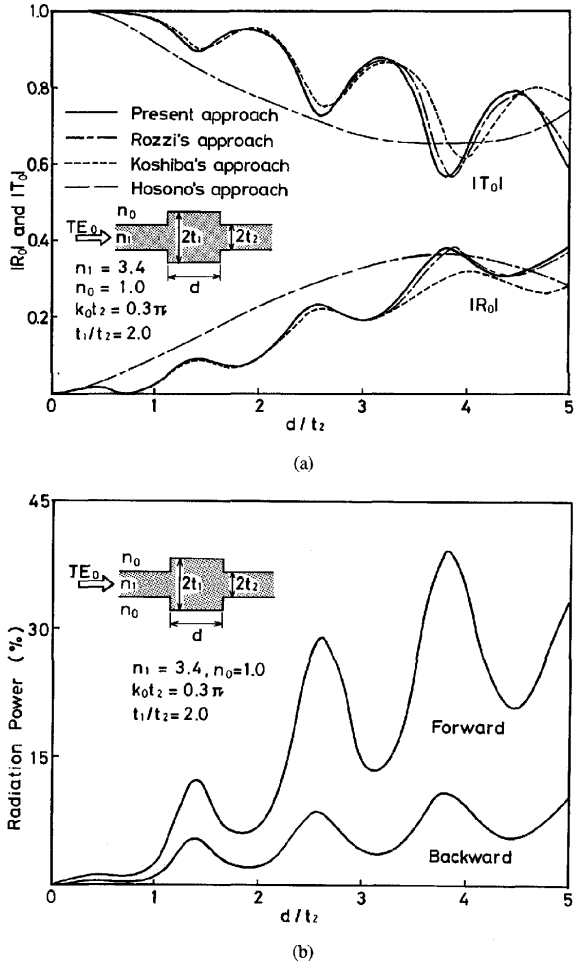

Figure 9. Numerical results of symmetric double-step: (a) Reflection and transmission coefficients, and (b) Radiation powers versus the rib width.

Comparative discussions among those approaches and results are presented in detail in [6]. For a more precise comparison, the radiation power must be calculated, but our method is one that calculates it. The results, shown in Fig. 9(b), exhibit an oscillatory nature corresponding to that seen in Fig. 9(a), and the radiation maxima just coincide with the oscillation maxima of R_0 , and the minima of T_0 in our results.

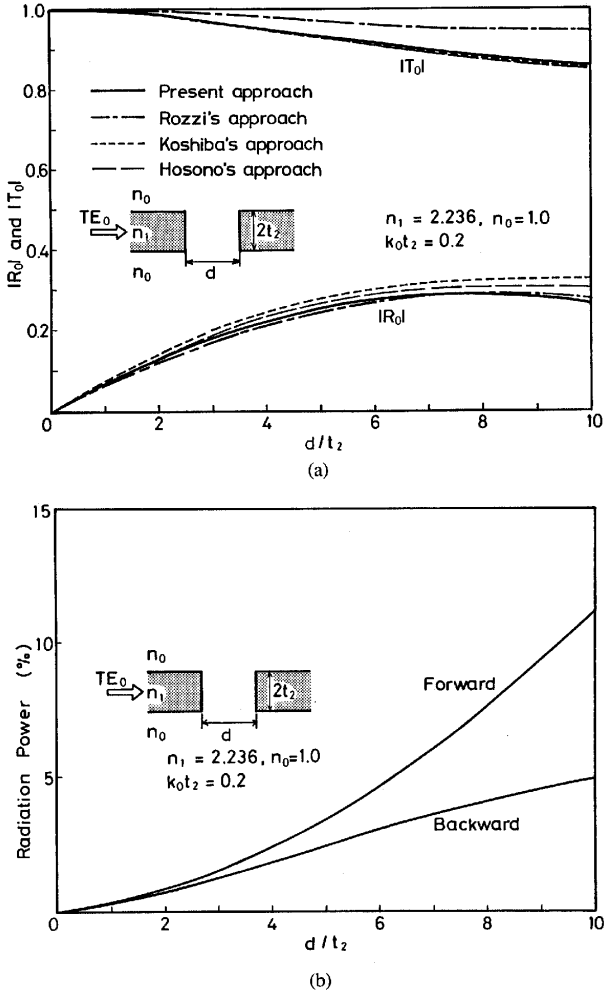

Figure 10. Numerical results of symmetric double-step with an air gap: (a) Reflection and transmission coefficients, and (b) Radiation powers versus the gap width.

On the other hand, the radiation powers shown in Fig. 10(b) monotonically increase with increasing d/t_2, corresponding to similar features of R_0 and T_0 in Fig. 10(a). Incidentally, our calculations presented here have been made with an error of about 0.5% or less in the power conservation relation at around $d/t_2 = 10$.

3.2 Mode Propagation through Periodic Corrugations with Finite Length.

Let us next consider the periodic dielectric corrugations of finite length shown in Fig. 11(a). This structure is given by the cascade connection of a finite number of networks given by Figs. 2 and 4, and we can derive the overall equivalent network for Fig. 11(a) by connecting repeatedly such constitutive networks expressed by the matrices $[S_{STEP}]$, $[S'_{STEP}]$ and $[S_{LINE}]$ or the finite cascades of the equivalent network shown in Fig. 7(b). The result is shown in Fig. 11(b).

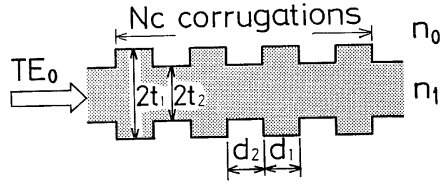

(a)

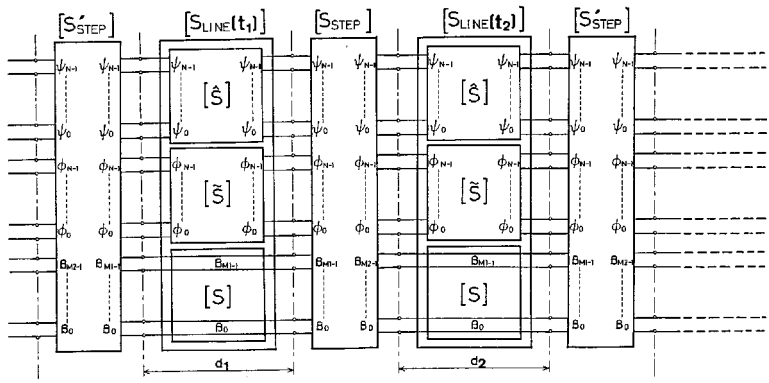

(b)

Figure 11. Periodically corrugated structure with finite length: (a) The configuration on the longitudinal section and equivalent network which is obtained by the finite cascades (b) Its of the equivalent network shown in Figure 7(a).

Applying the calculation procedures mentioned in Sec. 3.1, we can obtain the numerical results shown in Fig. 12, for a structure with the dimensions indicated in the inset and for a different number of corrugations N_c. The only surface-wave mode propagating in each homogeneous waveguide section is the TE_0 fundamental surface-wave

mode and we consider that this mode is incident from the left-hand side on the structure. Figure 12(a) shows the reflected power of the TE_0 surface-wave mode in the case where $N_c = 10$ and 20 corrugations, as a function of the normalized period $2d/\lambda_0$ while Fig. 12(b) shows the forward and backward radiation powers. If the structure under consideration is infinite in length, the first Bragg reflection occurs in the limited range of $2d/\lambda_0$ between 0.398 and 0.414, while the power radiation into space occur only in the leaky-wave region beyond $2d/\lambda_0 = 0.448$ for the present case. Figure 12(a) shows a strong reflection at around $2d/\lambda_0 = 0.406$ that corresponds to the center frequency of the first Bragg reflection region. Although the significant radiation indeed occurs in the leaky wave region, there are many subsidiary reflection peaks of the surface-wave mode even in that region and also the radiation still occurs in the first Bragg reflection region with a complicated feature arising from the finiteness of the periodic structure in length or due to "edge effect" [17].

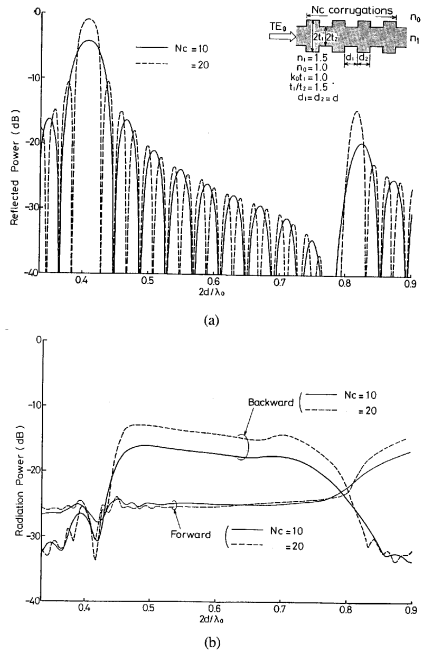

Figure 12. Numerical results for the periodic structure with finite length or with a finite number N_c of corrugations: (a) Reflected power of the incident TE_0 mode and (b) Radiation powers versus the normalized period $2d/\lambda_0$.

Now, as it is obvious in Fig. 12(b), the predominant radiation occurs in the backward direction which lies in the leaky-wave region. The radiation patterns calculated by the SDP approximation are shown in Fig. 13 for structures with $2d/\lambda_0 = 0.477\,,\ 0.516\,,$ and 0.577 in the case where $N_c = 10$ and $20\,$. The peak value is normalized to unity for each radiation pattern, and the axes along $\theta_{max} = 0°$ and $90°$ coincide with the y and the negative z directions, respectively. The effect of the finite length is indeed clearly seen in narrowing the main lobe as the number of corrugations increases, but more significantly, such an effect results in complicated spurious lobes. However, the direction of each maximum lobe is in good agreement with the angle calculated from the -1 st order space-harmonic wave in the structure extended infinitely ($\theta_{max} = 30°$ for Fig. 13(a), $45°$ for (b), and $60°$ for (c)).

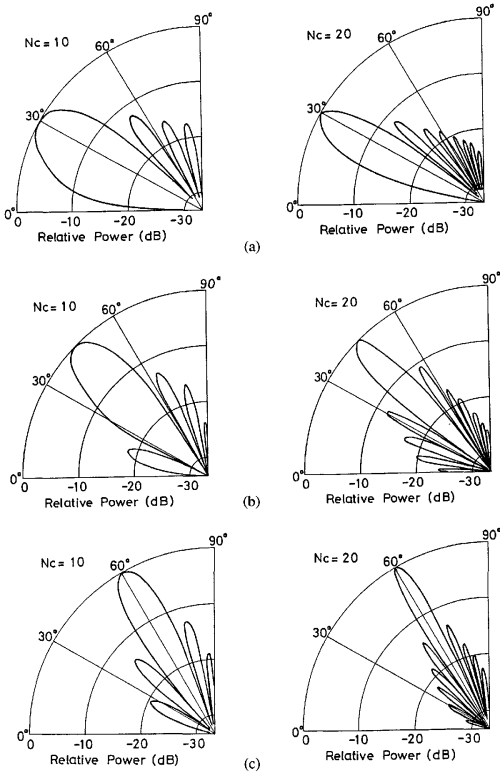

Figure 13. Backward radiation patterns from the periodic structure with a finite number of corrugations N_c: (a) The normalized period $2d/\lambda_0 = 0.477$, (b) $2d/\lambda_0 = 0.516$, and (c) $2d/\lambda_0 = 0.577$.

3.3 Low-Loss Design of Dialectric-Waveguide Y Branch.

Let us next discuss rather practical devices ranging from millimeter-wave to optical frequencies. Of these circuits, the Y branch is one of the basic but most important devices. It is used not only as a power divider and combiner, but also in the active devices for light-intensity modulation and switching. However, the guided wave on a Y branch always loses energy by radiation because of the discontinuous feature of branch structures. Such a radiation causes serious problems in circuit performance because of, for example, the undesired power coupling, or crosstalk, with neighboring circuits. Such an effect becomes significant in the millimeter-wave region, because branch circuits must be designed to be as compact as possible to the wavelength even if the junction angle becomes large and the dielectric constant ratio between the core and the surroundings increases.

Many approximate studies have been appeared so far (see the references of [18]). None of these studies, however, discussed the synthesis of Y branches by considering the accurate behavior of both the surface-wave mode and the radiation wave. It has been a common understanding that, once the radiation wave is generated, it is scattered to the surroundings and such a scattered wave cannot be used in devising low-loss Y branches. According to this view, a low-loss Y branch may be obtained only when the taper shape changes smoothly so that the input surface-wave mode can couple to the radiation wave as little as possible. This idea usually requires a large dimension to the wavelength for the nonuniform taper section, and such a Y branch will not be practical in the millimeterwave region.

In this section, we show a synthesis method of Y branches with amazingly reduced loss from radiation, which is based on our equivalent network approach. In a new type of Y branch, the radiation wave is intentionally generated along the taper and is controlled so that it can play an important role in reducing radiation loss (theoretically realizing zero loss) [19].

Figure 14 illustrates the Y branch considered in the analysis. For simplicity, the structure is assumed to be uniform in the x direction, and the fundamental TE_0 slab surface-wave mode is incident from the left-hand side of the waveguide as shown. Also, the separation of the output guides II and $\overline{II}$ is assumed to be sufficiently wide so that their effect on each other can be neglected. We assume further that each guide can support only the fundamental surface-wave mode.

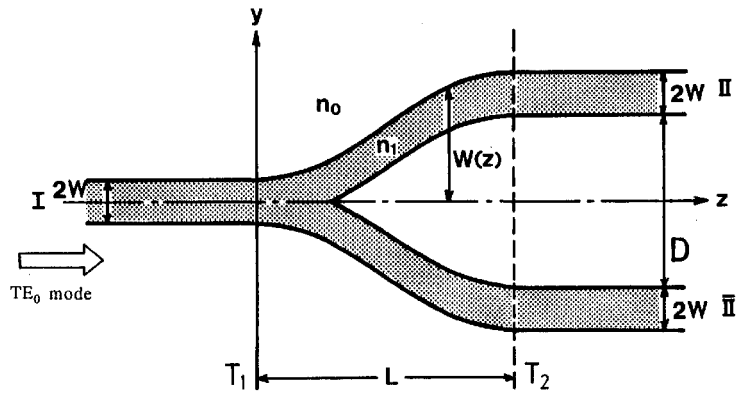

Figure 14. General configuration of dielectric waveguide Y branch. The structure is uniform in the x direction. The non-uniform structure lies between the terminal planes T_1 and T_2 which are connected to the input waveguide I and to the output waveguides II, $\overline{II}$, respectively.

As mentioned in Sec. 2.1, the electromagnetic field in a uniform dielectric waveguide of the open type can be expressed completely by the constituent fields of both the surface-wave modes and the radiation modes. The constituent modes do not couple with each other as long as a waveguide is uniform along the direction of propagation. However, if a waveguide becomes nonuniform as seen in Fig. 14, the power coupling occurs between surface-wave and radiation modes. Papers previously published have considered that a low-loss Y branch is obtained only when the transmitting power of the surface-wave mode is lost gradually along the taper axis and drops monotonically to a certain amount at the output end, marked T_2 as shown conceptually by the dashed curve Ⓐ in Fig. 15. This understanding is not correct, as explained below, when a Y branch in the millimeter-wave region is concerned.

It is obvious that the surface-wave mode on a practical Y branch propagates toward the output end, successively repeating, to a greater or lesser degree, the necessary power conversion and reconversion with the radiation modes as well as with the surface-wave mode. Then, it is expected that the power of the surface-wave mode will no longer change monotonically but rather in a more complex manner. Certainly, a numerical example for the practical linear-taper Y branch discussed later exhibits such a power change, not like curve Ⓐ but like curve Ⓑ in Fig. 15.

Figure 15. Conceptual variation of the transmitting power of the surface-wave mode across a plane perpendicular to the z axis.

Curve Ⓑ in Fig. 15 shows a sudden power conversion into the radiation modes near the input end, and then the power of radiation modes is again reconverted gradually into the surface-wave mode as they propagate. But, the power drop of the surface-wave mode at the output end T_2 is inevitable because a taper shape is decided *a priori*. Therefore, such a Y branch is always accompanied by a loss due to radiation. However, we can obtain a Y branch with theoretically no loss from radiation when the taper shape is designed so as to control intentionally the intensive power conversion and reconversion. Such a Y branch will transform a part of the input surface-wave mode into the radiation modes with complete control, and we can finally obtain only the desired surface-wave mode in the output waveguide, while the undesired reflection is suppressed at the input end. In such an ideal case, we may expect conceptually the power change shown by the solid curve Ⓒ in Fig. 15.

To control intentionally the power conversion and reconversion in a fashion mentioned above, it is necessary to solve the wave behavior on a Y branch from the viewpoint of a precise boundary-value

problem. For this purpose, we approximate a Y branch by a number of infinitesimal step discontinuities connected in tandem through a uniform dielectric waveguide with a segment length Δl_i as shown in Fig. 16. Such an approximated structure is then typically divided into four building blocks. The first (Fig. 17(a)) is the single homogeneous waveguide with guide width w_i, the second (Fig. 17(b)) is the step discontinuity on it, the third (Fig. 17(c)) is the parallel homogeneous waveguide with guide width w_i and separation d_i, and the last (Fig. 17(d)) is the step discontinuity. According to the results described in Sec's 2.1 and 2.2, part (a) and part (c) (homogeneous waveguides) of Fig. 17 can be expressed basically by the equivalent network of Fig. 1, denoted by $[S_{LINE}]$, while the equivalent network of Fig. 4, denoted by $[S_{STEP}]$ or $[S'_{STEP}]$, is used for expressing both part (b) and part (d) of Fig. 17, except for the difference in the functional forms of modal functions. As for part (c) and part (d), the surface-wave and radiation modes should be, of course, expressed in terms of the even type of modal functions in a parallel dielectric-slab waveguides.

As a result, the approximated structure Fig. 16 is understood as a cascade connection of all of the building blocks shown in Fig. 17, and the schematic draw of the equivalent network shown in Fig. 18 can be used for expressing the structure of Fig. 16. The network parameters expressing completely each of the elementary networks can be controlled by varying each of the guide widths w_i, the separation widths of parallel waveguides d_i and the segment lengths Δl_i $(i = 1, 2, \ldots, K)$. As was assumed at the beginning of this section, the only surface-wave mode on each output waveguide II or $\overline{II}$ is approximately the TE_0 mode, so that the surface-wave field on the branched output waveguide is mathematically expressed by the fundamental even TE surface-wave mode on a parallel dielectric slab. The insertion loss between input and output surface-wave modes is then expressed as a function of the variables $\{w_i, d_i, \Delta l_i\}$ $(i = 1, 2, \ldots, K)$, and they are solved by minimizing (ideally by making zero) the insertion loss at least at a given frequency by using a nonlinear optimization procedure. In this calculation, we set the constraint conditions that the resultant field transforms only into the desired surface-wave mode on the output waveguide with zero insertion loss, while keeping the total length L of the Y branch and the separation width D of two waveguides at the output end constant. In a practical design, we fix all of the guide widths w_i to W and the separation width D at the output end to $10W$. For the sake of

experimental convenience, a design is tried at the X band, by using the polyethylene $(n = 1.5)$ as a dielectric material. Numerical convergence has been checked, and it is found that the step's number of $K > 48$ is sufficient for approximating a Y branch in the form shown in Fig. 16 [5]. Therefore, the calculations hereafter are performed with $K = 48$. A total power conservation greater than 99.5 % is then achieved in the calculations.

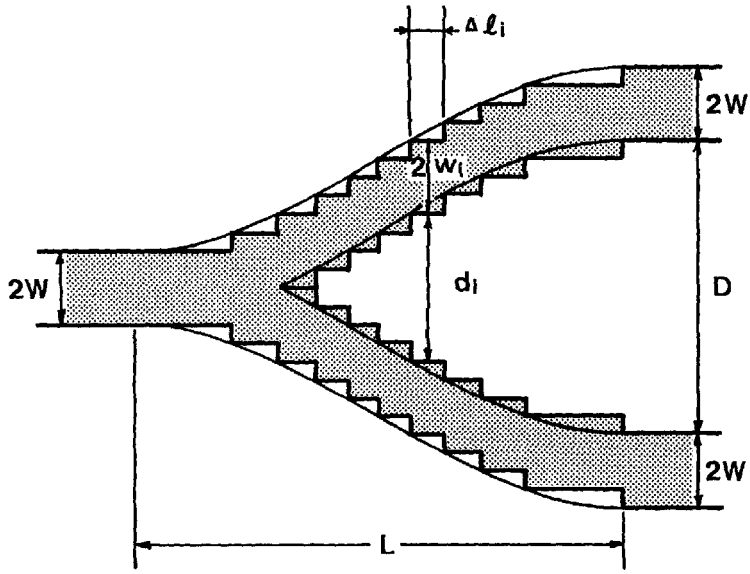

Figure 16. Step approximation for dielectric waveguide Y branch. Its original shape is indicated by the smooth curve (The sketch is exaggerated.).

Let us here synthesize a low-loss Y branch at $k_0W = 1$ and with $n = 1.5$ by varying each of the segment lengths Δl_i, while keeping $L = 15W$. The segment lengths Δl_i are then solved by the modified Newton iteration method. Figure 19(a) shows the Y branch synthesized at 9.55 GHz (which corresponds to $k_0W = 1$ when $W = 5mm$), and the calculated insertion loss of this new Y branch is $0.32dB$ at that frequency. Further, the ratio of power division into both output ports is 1.0. The configuration of Fig. 19(a) consists of the serpentine taper and the abrupt step at both input and output ends. This result indeed seems to be an unexpected one from the usual design point of view, but the prudential physical consideration explains that this result is

certainly consistent with our original idea. For example, the solid curve in Fig. 19(b) shows the calculated power change of the local surface-wave mode for the synthesized Y branch, while the dashed curve shows that for the linear-taper Y branch which has the same dimensions as Fig. 19(a) except that the serpentine taper is replaced by a linear taper. As expected, the synthesized Y branch certainly improves the power drop of the surface-wave mode at the output end, and exhibits the low-loss nature. But, the solid curve is somewhat different from that of the ideal case ⓒ in Fig. 15 and there is a small amount of the residual loss. This can be removed when each of the guide widths w_i is also considered as a variable along with Δl_i [20]. However, the computing time increases, and the design cost becomes a bit high.

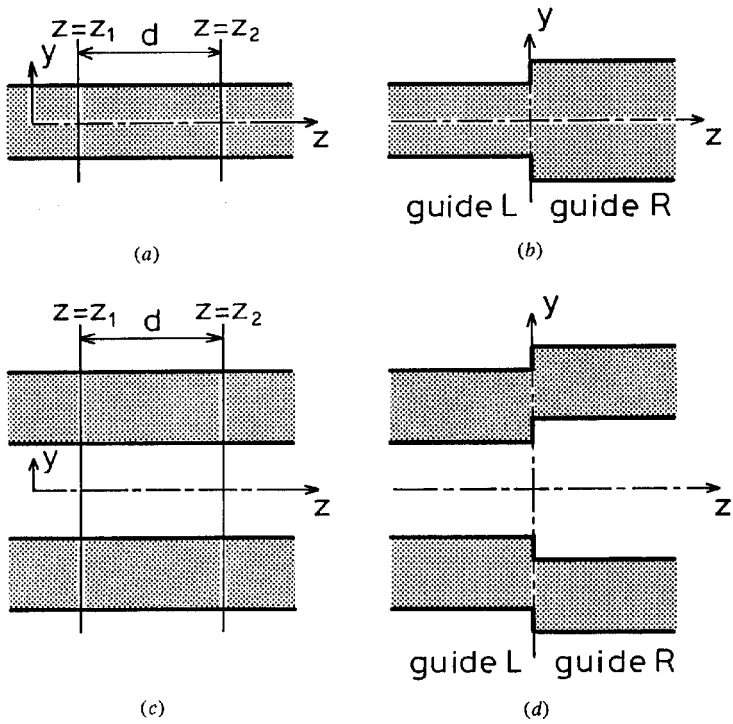

Figure 17. Typical four types of building blocks composing the approximated structure of Figure 16; (a) the single homogeneous dielectric slab, (b) the step discontinuity on the waveguide shown in (a), (c) the parallel homogeneous dielectric slab, and (d) the step discontinuity on the waveguide shown in (c).

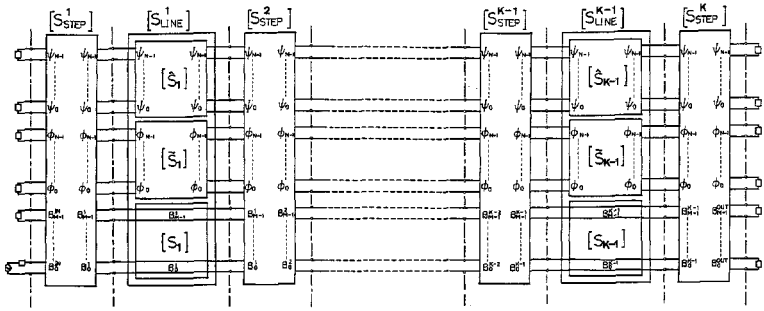

Figure 18. Equivalent network representation for dielectric waveguide Y branch with an arbitrarily shaped taper. The network parameters are controlled by varying each of guide width w_j, the separation width of parallel waveguides d_i, and the segment lengths Δl_i in Figure 16.

We performed a set of measurements on a synthesized Y branch at $f = 9.55$ GHz. The dielectric was polyethylene, with $n = 1.5$; the guide width W was 5 mm, the length of the taper section was $L = 15W = 75mm$, and the branch was made by a numerically controlled machine. This test branch was placed in a parallel-plate waveguide with separation of 8mm to simulate a two-dimensional structure. An external view of a synthesized Y branch for test is shown in Fig. 20(a). Figure 20(b) shows the measured insertion loss characteristics as a function of frequency. The dotted circles indicate the calculations for the Y branch of Fig. 19(a), while the solid curve shows the measured characteristic. It is seen that the measured insertion loss agrees excellently with the calculated one (0.32 dB) at $f = 9.55$ GHz. This corresponds to the fractional power of 93% of input surface-wave mode transmitted to the output waveguides. Figure 20(b) also presents another set of calculations and experiment. The single circles indicate the calculation for the linear-taper Y branch which has the same dimension with that of Fig. 19(a). In this case, the insertion loss at $f = 9.55$ GHz is about $0.85dB$, which is 2.7 times worse than the insertion loss of the serpentine-taper Y branch. We can also confirm that the serpentine-taper Y branch shows low-loss characteristic over a wide frequency range, although the optimization is performed at the frequency $f = 9.55$ GHz.

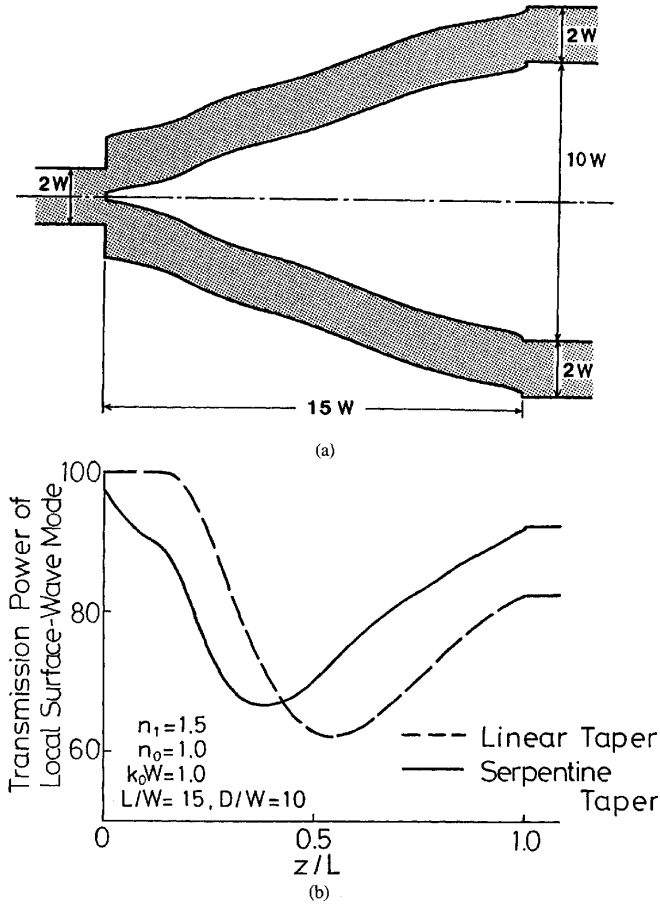

Figure 19. Characteristic features of the low-loss Y branch synthesized at $k_0W = 1$: (a) Configuration of the low-loss Y branch (not exaggerated, but enlarged in its scale), and (b) Curve of the calculated power change of the surface-wave mode with the comparative one for the linear-taper Y branch.

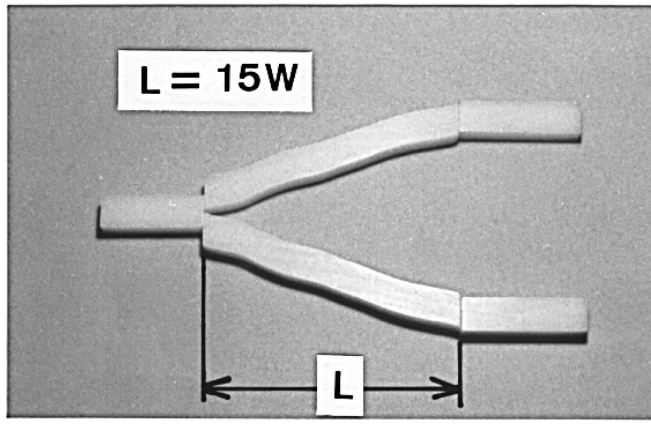

(a)

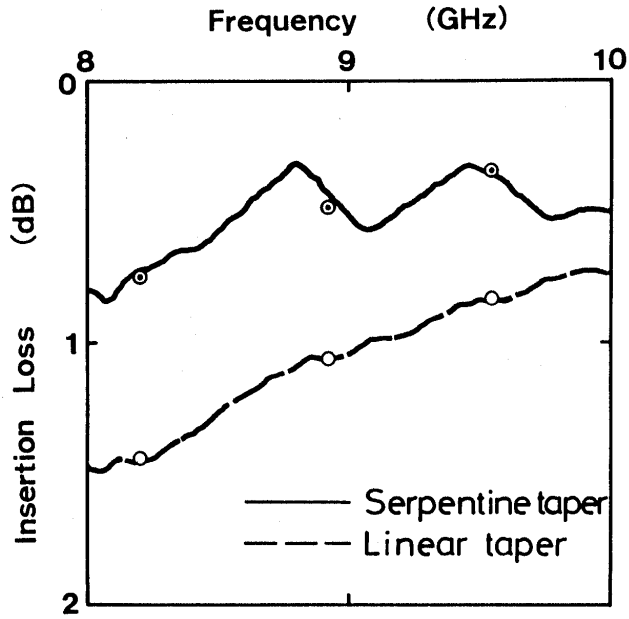

(b)

Figure 20. Experimental results of the synthesized Y branch; (a) The external view of the Y branch for test, and (b) Curves of the insertion loss as a function of frequency for the synthesized Y branch and for the linear-taper Y branch. The synthesis is performed at $f = 9.55$ GHz.

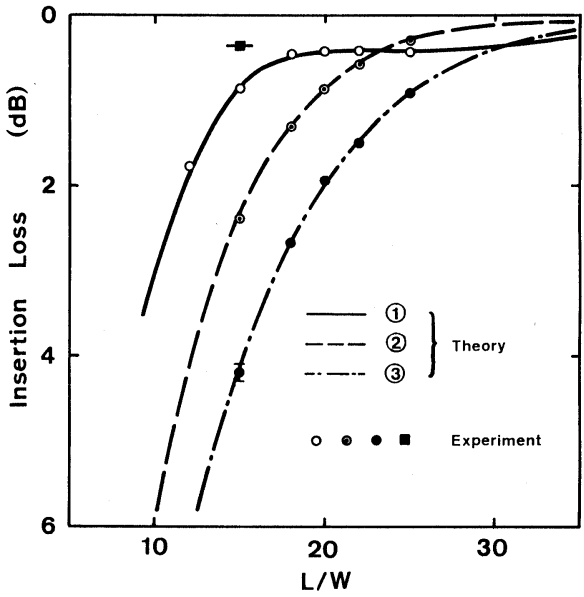

Figure 21. Calculated and measured insertion loss as a function of the normalized taper length L/W for the Y branches with the linear taper ①, the raised-cosine taper ②, and the integrated raised-cosine taper ③. The square mark on $L/W = 15$ indicates the insertion loss of the synthesized Y branch.

As comparative branch structures, we have also investigated the Y branches with the raised-cosine and integrated raised-cosine tapers for which the first and the second derivatives are continuous at the junction points, respectively [21–22]. These are often used in the optical region. Figure 21 shows the calculated and measured characteristics of the insertion loss as a function of the normalized taper length L/W along with those for the linear-taper Y branch. These calculations have also been performed by the equivalent network approach followed in the numerical synthesis. For comparison, the measured loss of the synthesized low-loss Y branch at $L/W = 15$ is also shown by the square mark. These results are also summarized in Table 1 along with reflected power, backward and forward radiation powers. It is seen from these results that the radiation loss of the raised-cosine and integrated raised-cosine taper Y branches is much larger than that of the linear taper when they are designed compactly to the wavelength, for example, in the region of $L/W < 20$. This is understood from the fact that,

since the design idea of such Y branches undertakes only a smooth mode conversion between surface-wave modes on the input or the output waveguide and those on the taper section. A large loss is inevitable when the total length of a Y branch is shortened and the bend around the junctions becomes sharp.

Kinds of Y-branch	reflected power	trans-mission power	Backward radiation power	Forward radiation power	Total power
Low-loss Y-branch	0.00	92.45	0.58	6.30	99.33
Linear taper	0.01	82.63	0.35	16.46	99.44
Raised cosine taper	0.05	58.02	0.62	39.99	98.69
Integral raised-cosine taper	0.17	38.74	1.03	58.09	98.03

(The power is shown in per cent.)

Table 1. Comparison of the calculations of typical Y-branch characteristics ($L = 15W$).

The low-loss nature of the serpentine-taper Y branch is also confirmed from the wave behavior around the taper section. Figure 22(a) shows the field intensity distribution for the serpentine-taper Y branch with $L/W = 15$, while parts (b), (c) and (d) show the distributions for the Y branches with linear taper, raised-cosine taper and integrated raised-cosine taper of the same L/W, respectively. It is clearly seen that the serpentine taper Y branch smoothly transforms the input surface-wave mode into the surface-wave mode on the output waveguide with the help of the local radiation wave, as we expected. In contrast to this, Y branches with conventional tapers scatter the radiation wave away from the Y branch. This tendency is remarkable for the case of tapers with a smooth transition on their configurations, such as the raised-cosine tapers. Consequently, the performance of the newly designed Y branch is superior to other branches whose shapes are defined *a priori*, and the method described here can evidently be very effective for designing low-loss Y branch in the millimeter-wave region.

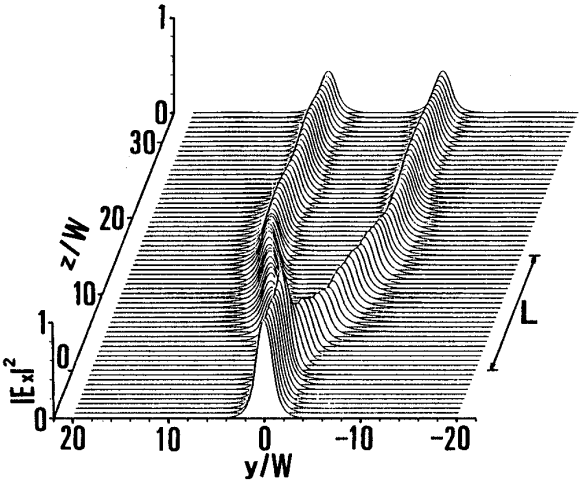

Figure 22(a). Field intensity distribution around the taper section with $L/W = I5$ for the synthesized serpentine-taper Y branch when only the surface-wave mode is incident from the $-z$ direction.

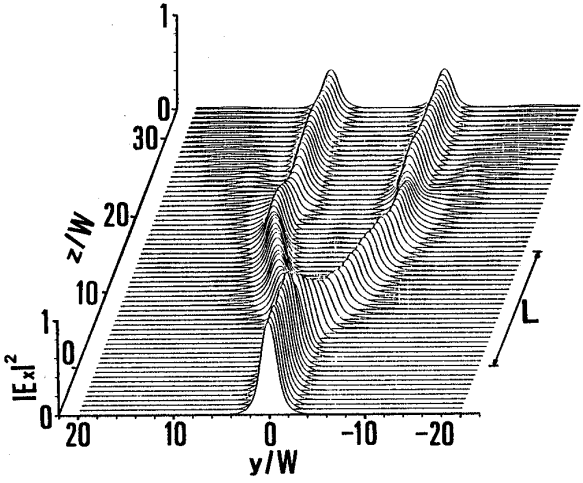

Figure 22(b). Field intensity distribution around the taper section with $L/W = 15$ for the linear-taper Y branch when only the surface-wave mode is incident from the $+z$ direction.

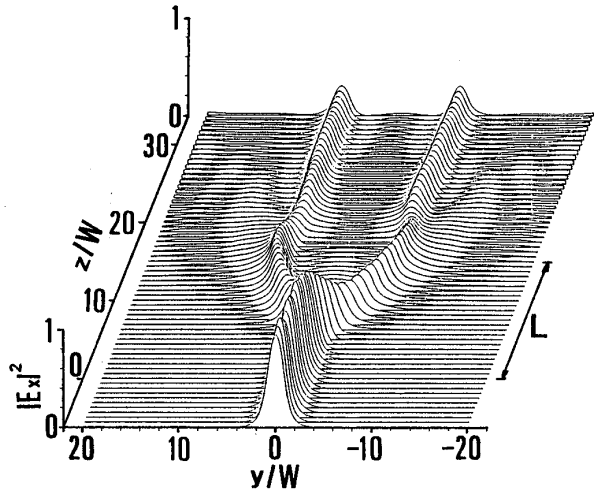

Figure 22(c). Field intensity distribution around the taper section with $L/W = 15$ for the raised-cosine taper Y branch when only the surface-wave mode is incident from the $-z$ direction.

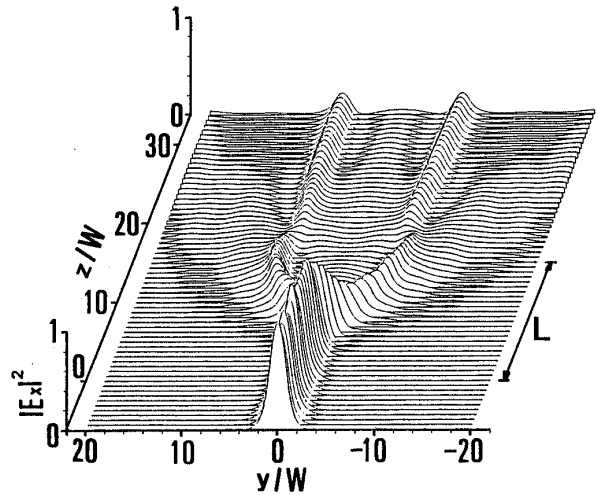

Figure 22(d). Field intensity distribution around the taper section with $L/W = 15$ for the integrated raised-cosine taper Y branch when only the surface-wave mode is incident from the $-z$ direction.

4. Electromagnetic-Wave Scattering and Diffraction

4.1 Equivalent Network for Discontinuity in Space.

In this section, we demonstrate that our equivalent network approach is quite effectively applied to electromagnetic-wave scattering and diffraction problems [23]. Among those problems, our approach is specially suited to analyze finite array of conducting or dielectric strips (or unit cells) which are illuminated by an incident space wave. These structures are extensively used as polarization-selective surface, frequency selective surface and so on. The analyses of these structures are often carried out under the assumption that they are infinite in length (see the references of [24,25]), even if the dimensions of practical structures are necessarily finite. On the other hand, the integral equation method is widely used for analyses of such finite problems, in which the integral operator is usually transformed into either the spatially algebraic operator [26] or the spectral one [24]. These approaches then require the handling of a large number of unknowns in numerical calculations when practical structures comprise a large, but finite number of unit cells, and a few approaches [24,27-29] have challenged to relax some of practical difficulties caused by the prohibitively large storage on the computer.

Our approach is perfectly different from those ones as it is clear from the discussions in the previous sections, and can greatly relax the computational difficulties still existing in the approaches just mentioned above, because our approach applied to scattering problems starts also from the partition of structures into several kinds of basic building block, and expresses the electromagnetic-wave behavior in each of them by one of appropriate equivalent network matrices derived in Sec. 2. By the way, we should discuss here the junction-discontinuity problem that is left in Sec. 2.3. It is to derive the equivalent network matrix that expresses the wave behavior at the half-space open end which is a junction between a half space and a full space as shown in Fig. 23.

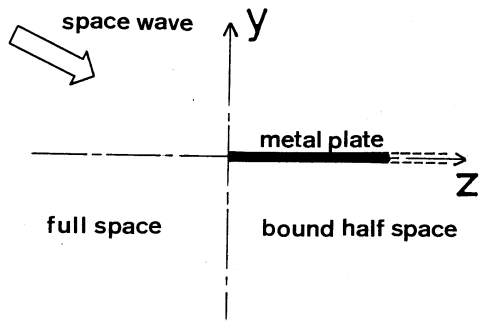

Figure 23. Discontinuity configuration of a half-space open end that is a junction discontinuity between a half space bound by an electrically conducting plate and a full space.

Now, let us consider, without loss of generality, that the bounded half space is realized by a conducting semi-infinite plate with zero thickness, placed on the xz plane at $y = 0$. There is no dielectric waveguide, so that the fields in either side consist only of the spectral composite modes. Let us assume here that an arbitrary excitation wave poralized in the x direction is incident with an arbitrary slant angle from the full space region (the left-hand side ($z < 0$)) as shown in Fig. 23. Since the structure of Fig. 23 is symmetric with respect to the xz plane at $y = 0$, such an excitation problem can be divided into two consistent problems; one (we call it the problem A) is characterized by the constituent E_x component with the antisymmetric distribution with respect to the xz plane at $y = 0$ and the other (the problem B) is characterized by that with the symmetric distribution with respect to that symmetry plane. For the problem A, we may replace the symmetry plane with the short circuit over the full range of z, and it turns out that the problem A is equivalent to a simple problem that the antisymmetric constituent of fields is perfectly reflected by the short circuit or electrically conducting plane extending uniformly on the xz plane at $y = 0$. Therefore, this constituent problem A does not include any type of junction discontinuities on the xy plane at $z = 0$, and also we have only to consider the odd type of the spectral composite modes with respect to the xz plane at $y = 0$. Thus, the terminal port for one of odd spectral-composite modes on the z_- side of the junction is directly connected to the corresponding terminal port on the z_+ side without any discontinuity matrix.

On the other hand, for the problem B, the fields are characterized by the constituent E_x component with the symmetric distribution with respect to the xz plane at $y = 0$ over the full range of z. In this case, we may introduce an open-circuit condition on such a symmetry plane and we have only to consider the even type of spectral composite modes with respect to the xz plane at $y = 0$. However, the structure at the present case is not uniform along the z-axis, but the free space is extended in the region of $z < 0$, while the one for $z > 0$ is occupied by the semi-infinite space bound by an electrically conducting plane. Therefore, the problem B necessarily includes a junction discontinuity at the xy plane at $z = 0$, and we should consider that the E_x field distribution along the y axis is the type of $\cos(\rho y)$ for $z < 0$, while it is the type of $|\cos(\rho' y)|$ for $z > 0$. By considering these different types of even modal function in the regions $z < 0$ and $z > 0$, and by applying the field-continuity conditions at the xy plane at $z = 0$ as seen in Sec. 2.3, we can obtain the junction matrix $[S_D^a]$ for the present case as shown in Fig. 24. With the same procedures, another matrix $[S'^a_D]$ can be obtained, which is used for the structure of the mirror inversion of Fig. 23 with respect to the xy plane at $z = 0$.

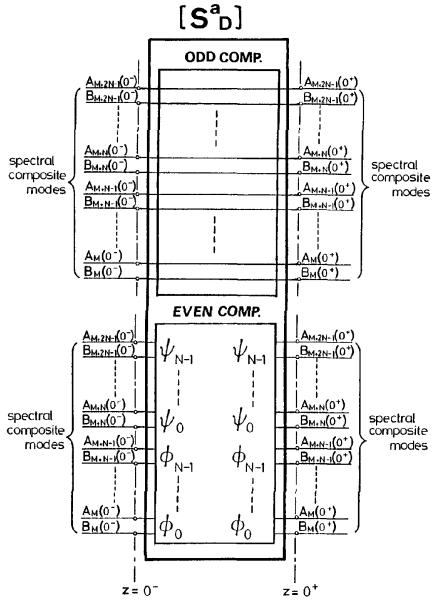

Figure 24. Equivalent network representation $[S_D^a]$ for a half-space open end shown in Figure 23.

4.2 Scattering from Finite Array of Conducting Strips.

To understand how to apply our approach to scattering problems, let us consider an array of conducting strips with zero thickness as shown in Fig. 25(a). This structure is partitioned into four building blocks by correctly defining the terminal planes as shown. There are two junction discontinuities, one zonal half space of length l_i and one zonal full space of width d_j , ($i, j = 1, 2, \ldots, M$). By following the matrix notation for each constituent structure mentioned above or in Sec. 2.3, those building blocks can be expressed by the equivalent matrices $[S^a_D]$, $[S' a_D]$, $[S^h_{ZONE}]$ and $[S^f_{ZONE}]$. Thus, by connecting properly these matrices in tandem, the overall equivalent network is obtained as shown in Fig. 25.

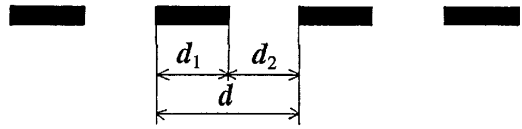

(a)

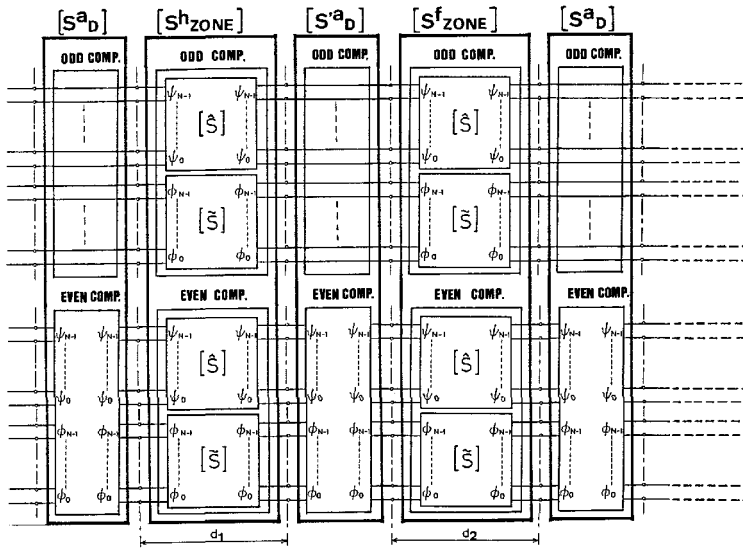

(b)

Figure 25. Finite array of conducting strips; (a) The configuration on the longitudinal section, and (b) Its equivalent network.

In our approach, on the other hand, the incident Gaussian wave beam is expanded in terms of the spectral composite modes on the plane T_1, the most left end of the structure in Fig. 25(b), and such a known amplitude of each mode is considered to be an equivalent-source amplitude impressed at each terminal port on that plane. Then, in this sense, there is no impressed source at all of the terminal ports on the output plane T_2, the most right end of the structure, so they should be terminated with the appropriate matched impedances for spectral composite modes as shown. By solving this equivalent network problem with impressed sources, we can obtain the resulting amplitudes of the outgoing spectral composite modes at both output and input terminal ports. Thus, by reconstructing the radiation fields on the terminal planes from these known amplitudes and applying the SDP approximation, we can approximately calculate the fields radiated in both forward $(+z)$ and backward$(-z)$ directions.

Let us assume here that the array is illuminated by an Gaussian wave beam incident only from the upper side with a slant angle $15°$. Figures 26 and 27 show the scattering fields for the incident wave with the beam waist $w_0/\lambda_0 = 4.0$ and the beam offset $x_0/\lambda_0 = 0$, when the number of conducting strips M is varied.

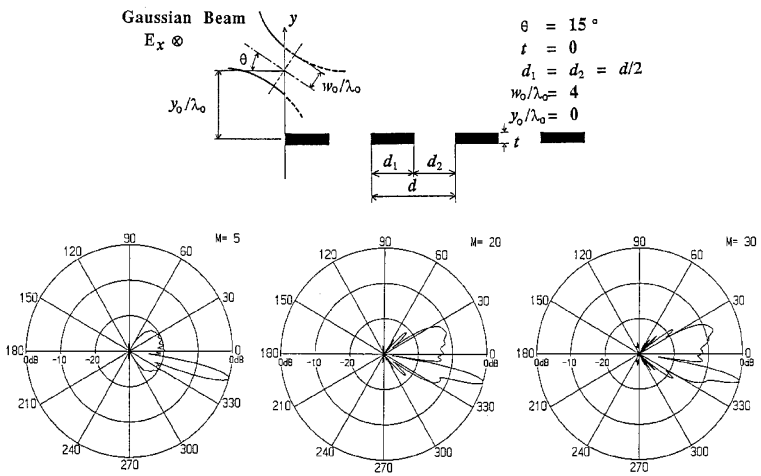

Figure 26. Scattering patterns calculated for the incident Gaussian beam, when the number M of conducting strips is varied. This case is $k_0 d/2 = 1.0$ so that no diffraction angle satisfies the Bragg condition of the infinite array.

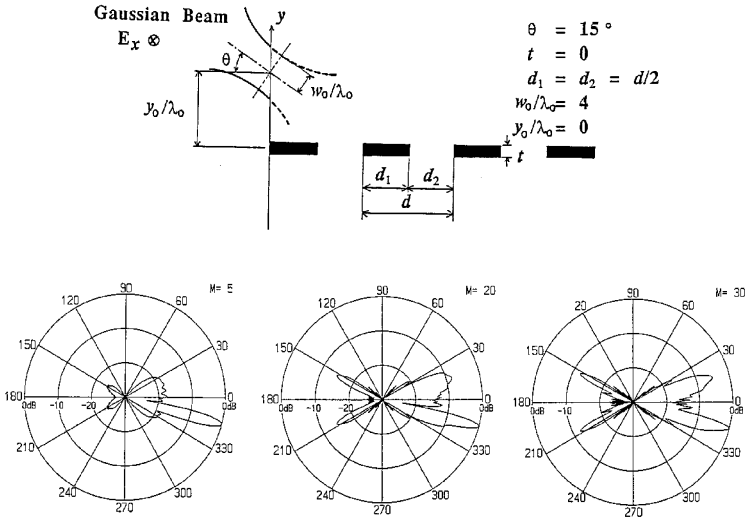

Figure 27. Scattering patterns calculated for the incident Gaussian beam, when the number M of conducting strips is varied. This case is $k_0 d/2 = 1.715$ so that the backward radiation occurs to the Bragg reflection angles given by $150°$ and $210°$.

Since the separation d of conductor strips in the case of Fig. 26 is chosen as $k_0 d/2 = 1.0$, any diffraction angle does not theoretically satisfy the Bragg condition. While, d of Fig. 27 is chosen as $k_0 d/2 = 1.715$ so that the incident wave is scattered back to the directions of the angles given by $150°$ and $210°$, which correspond just to the Bragg reflection angles of the -1 st order space-harmonic if the strips are arrayed infinitely with the same period.

We can see from Fig. 26 that the array with a small number of strips (e.g., $M = 5$) transmits most of the incident power to the same direction and the reflected wave from the plane of the array surface increases in its intensity as M increases. While, the backward diffraction does not occur in this case as expected. On the other hand, Fig. 27 shows that the radiation peaks of backward diffraction clearly appear at the expected Bragg-reflection angles and their intensity monotonically increases with increasing M. Obviously, these results consist of very complicated subsidiary peaks which arise from the finiteness

of the array in length, or the "edge effect". Such detailed results are certainly obtained by our approach.

Although only few numerical results are presented here, these results show that the present method is a very useful and powerful approach to problems of scattering or diffraction from the finite arrays of conducting strips. The present approach is quite adaptive to structures, so that it is easy to solve problems, for example, that conducting strips or dielectric strips with different widths are arrayed aperiodically [30–32].

5. Concluding Remarks

In this chapter, a new equivalent network approach has been presented, which is powerful for investigating precisely the wave-guiding and wave-scattering natures of discontinuous structures with finite extent. This finiteness is indeed a very important feature of practical structures. However, its mathematical treatment, especially in efficient numerical approach, is quite difficult, and most of the published investigations have shunned discussing this problem neatly. In this chapter, we have initiated a breakthrough in surmounting this difficulty by a novel network approach which is based on the familiar equivalent network approach seen in closed waveguide problems, and have shown that this method is easy to use for microwave engineers. The present method has been successfully applied to devise other types of components [33-35] and also to design leaky-wave antennas based on dielectric-corrugations structures [36-37]. Although the structures discussed here have been two-dimensional structers, we have also been sucessful in applying the present method to more practical three-dimensional structures with the help of an unprecedented method for structural approximations. The readers who are interested in those structures will find data in [38-40].

Appendices

Appendix I

Let $h_{yk}(y)$ be the magnetic modal function associated with $e_{xk}(y)$. Then the orthonormal relations for the spectral composite modes are given as follows.

1. Relations Between the Spectral Composite Modes Belonging to the Same Regions of ρ

$$\begin{aligned}
&\int_{-\infty}^{\infty} \tilde{e}_{xn}(y)\tilde{h}_{yk}(y)dy \\
&\quad = \int_{-\infty}^{\infty} \left(\int_0^{n_0k_0} \phi_n(\rho)e_x(y,\rho)d\rho \right) \left(\int_0^{n_0k_0} \phi_k(\rho')h_y(y,\rho')d\rho' \right) dy \\
&\quad = \int_0^{n_0k_0} \int_0^{n_0k_0} \phi_n(\rho)\phi_k(\rho') \left(\int_{-\infty}^{\infty} e_x(y,\rho)h_y(y,\rho')dy \right) d\rho d\rho' \\
&\quad = \int_0^{n_0k_0} \phi_k(\rho') \left(\int_0^{n_0k_0} \phi_n(\rho)\delta(\rho-\rho')d\rho \right) d\rho' \\
&\quad = \int_0^{n_0k_0} \phi_n(\rho')\phi_k(\rho')d\rho' = \delta_{nk}
\end{aligned} \tag{A1}$$

2. Relations Between the Spectral Composite Modes Belonging to Different Regions of ρ

$$\begin{aligned}
&\int_{-\infty}^{\infty} \tilde{e}_{xn}(y)\hat{h}_{yk}(y)dy \\
&\quad = \int_{-\infty}^{\infty} \left(\int_0^{n_0k_0} \phi_n(\rho)e_x(y,\rho)d\rho \right) \left(\int_{n_0k_0}^{\alpha n_0k_0} \psi_k(\rho')h_y(y,\rho')d\rho' \right) dy \\
&\quad = \int_{n_0k_0}^{\alpha n_0k_0} \int_0^{n_0k_0} \psi_k(\rho')\phi_n(\rho) \left(\int_{-\infty}^{\infty} e_x(y,\rho)h_y(y,\rho')dy \right) d\rho d\rho' \\
&\quad = \int_{n_0k_0}^{\alpha n_0k_0} \psi_k(\rho') \left(\int_0^{n_0k_0} \phi_n(\rho)\delta(\rho-\rho')d\rho \right) d\rho' = 0
\end{aligned} \tag{A2}$$

3. Relations Between a Spectral Composite Mode and a Surface-Wave Mode

$$\begin{aligned}\int_{-\infty}^{\infty} \tilde{e}_{xn}(y) h_{ym}(y) dy &= \int_{-\infty}^{\infty} \left(\int_{0}^{n_0 k_0} \phi_n(\rho) e_x(y,\rho) d\rho \right) h_{ym}(y) dy \\ &= \int_{0}^{n_0 k_0} \phi_n(\rho) \left(\int_{-\infty}^{\infty} e_x(y,\rho) h_{ym}(y) dy \right) d\rho \\ &= 0 \end{aligned} \tag{A3}$$

Appendix II

The equivalent network of Fig. 2 for a homogeneous dielectric waveguide of length d is represented in the following matrix form of order $2M + 4N$:

$$[b][S_{LINE}][a] \tag{A4}$$

where

$$[S_{LINE}] = \begin{bmatrix} 0_{MM} & 0_{MN} & 0_{MN} & S & 0_{MN} & 0_{MN} \\ 0_{NM} & 0_{NN} & 0_{NN} & 0_{NM} & \tilde{S} & 0_{NN} \\ 0_{NM} & 0_{NN} & 0_{NN} & 0_{NM} & 0_{NN} & \hat{S} \\ S & 0_{MN} & 0_{MN} & 0_{MM} & 0_{NM} & 0_{NN} \\ 0_{NM} & \tilde{S} & 0_{NM} & 0_{NM} & 0_{NN} & 0_{NN} \\ 0_{NM} & 0_{NN} & \hat{S} & 0_{NM} & 0_{NN} & 0_{NN} \end{bmatrix} \tag{A5}$$

$$\begin{aligned}[a] = [&A_0(z_1), \cdots, A_{M-1}(z_1), A_M(z_1), \cdots, A_{M+N-1}(z_1), A_{M+N}(z_1), \\ &\cdots, A_{M+2N-1}(z_1), A_0(z_2), \cdots, A_{M-1}(z_2), A_M(z_2), \cdots, \\ &A_{M+N-1}(z_2), A_{M+N}(z_2), \cdots, A_{M+2N-1}(z_2)]^t \end{aligned} \tag{A6}$$

$$\begin{aligned}[b] = [&B_0(z_1), \cdots, B_{M-1}(z_1), B_M(z_1), \cdots, B_{M+N-1}(z_1), B_{M+N}(z_1), \\ &\cdots, B_{M+2N-1}(z_1), B_0(z_2), \cdots, B_{M-1}(z_2), B_M(z_2), \cdots, \\ &B_{M+N-1}(z_2), B_{M+N}(z_2), \cdots, B_{M+2N-1}(z_2)]^t. \end{aligned} \tag{A7}$$

$[0_{IJ}]$ means the zero matrix of the order $I \times J$ and the superscript t denotes transposition. $[\tilde{S}]$ and $[\hat{S}]$ are matrices of order N, the

elements of which are given by (11) and (13), respectively, while $[S]$ is a matrix of the order M corresponding to the surface-wave modes in (3), and its elements S_{mq} are given by

$$S_{mq} = \delta_{mq} e^{-j\beta_m d} \tag{A8}$$

Appendix III

The scattering matrix $[S_{STEP}]$ for the isolated step discontinuity is expressed as follows:

$$[b] = [S_{STEP}][a] \tag{A9}$$

where the definitions of $[a]$ and $[b]$ are the same as in (A6) and (A7) with z_1 and z_2 replaced by 0^- and 0^+, respectively. Let us first consider the case where only the qth surface-wave mode is incident on the step from the left-hand side with amplitude $A_q(0^-) = 1$ and otherwise zero ($A_p(0^-) = 0$ for $p \neq q$ and $A_p(0^+) = 0$ for all p). For this example, we can obtain $(2M + 4N)$ elements of S_{pq} ($p = 0, 1, \ldots, 2M + 4N - 1$) on the qth row of $[S_{STEP}]$ immediately from the coefficients R_{qp} and T_{qp} as follows:

$$S_{pq} = R_{qp} \qquad S_{M+2N+pq} = T_{qp} \tag{A10}$$

Following the same method for the incidence of each of the other modes from guide I or guide II, all of the matrix elements for the equivalent network shown in Fig. 4 are solved.

Appendix IV

The terminal impedance Z_n of the spectral composite mode in the radiative part of the continuous spectrum ($0 < \rho < n_0 k_0$) can be defined by

$$\tilde{Z}_n \tilde{h}_{yn}(y) = \tilde{e}_{xn}(y) = \int_0^{n_0 k_0} \left(\frac{\omega \mu_0}{\beta(\rho)} \right) \phi_n(\rho) h_y(y, \rho) d\rho \tag{A11}$$

Multiplying both sides by e_{xn} and using the orthonormal relation (Al), we obtain

$$
\begin{aligned}
&\tilde{Z}_n \\
&= \int_{-\infty}^{\infty} \left(\int_0^{n_0 k_0} \phi_n(\rho') e_x(y, \rho') d\rho' \right) \left(\int_0^{n_0 k_0} \frac{\omega \mu_0}{\beta(\rho)} \phi_n(\rho) h_y(y, \rho) d\rho \right) dy \\
&= \int_0^{n_0 k_0} \phi_n(\rho') \left(\int_0^{n_0 k_0} \frac{\omega \mu_0}{\beta(\rho)} \phi_n(\rho) \delta(\rho - \rho') d\rho \right) d\rho' \\
&= \int_0^{n_0 k_0} \frac{\omega \mu_0}{\beta(\rho)} \phi_n(\rho') \phi_n(\rho') d\rho'. \qquad \text{(A12)}
\end{aligned}
$$

In the same way, Z_n in the reactive part ($n_0 k_0 < \rho < \alpha n_0 k_0$) is obtained:

$$
\hat{Z}_n = -j \int_{n_0 k_0}^{\alpha n_0 k_0} \frac{\omega \mu_0}{\gamma(\rho')} \psi_n(\rho') \psi_n(\rho') d\rho'. \qquad \text{(A13)}
$$

References

1. Clemmow, P. C., *The Plane Wave Spectrum Representation of Electromagnetic Fields*, Oxford, Pergamon Press, 1966, Part I.
2. Lewin, L., *Advanced Theory of Waveguides*, London, Iliffe & Sons, 1951.
3. Schwinger, J., and D. S. Saxon, *Discontinuities in Waveguides*, New York, Gordon and Breach Science, 1968.
4. Shigesawa, H., and M. Tsuji, "Mode propagation through a step discontinuity in dielectric planar waveguide," *1984 IEEE/MTT-S Intern'l. Microwave Symp. Digest*, (San Francisco, CA), 7–17, May 1984.
5. Shigesawa, H., and M. Tsuji, "Mode propagation through a step discontinuity in dielectric planar waveguide," *IEEE Trans. Microwave Theory Tech*, Vol. MTT-34, 205–212, Feb. 1986.
6. Shigesawa, H., and M. Tsuji, "A new equivalent network method for analyzing discontinuity properties of open dielectric waveguides," *IEEE Trans. Microwave Theory Tech*, Vol. MTT-34, 205–212, Feb. 1986.
7. Shigesawa, H., and M. Tsuji, "A new modal expression of the fields on dielectric waveguides of open type," *1987 URSI Radio Science Meeting Digest*, (Blacksburg, VA), June 1987, pap. JB01-5.

8. Marcuse, D., *Light Transmission Optics (Second Edition)*, New York, Van Nostrand Reinhold, 1982, Ch. 8.
9. Morishita, K., S. Inagaki, and N. Kumagai, "Analysis of discontinuities in dielectric waveguides by means of the least squares boundary residual method," *IEEE Trans. Microwave Theory Tech*, Vol. MTT-27, 310–315, Apr. 1979.
10. Luenberg, D. G., *Optimization by Vector Space Methods*, New York, John Wiley & Sons Inc., 1969, Ch. 3.
11. Sommerfeld, A., *Partielle Differentialgleichungen der Physik*, translated into Japanese by H. Masuda, Tokyo: Kodansha, 1986.
12. Elachi, C., "Waves in active and passive periodic structure: A review," *Proc. IEEE*, Vol. 64, 1666, 1698, Dec. 1976.
13. Kajfez, D., and P. Guillon, Edit., *Dielectric Resonators*, Dedham: Artech House, 19867, Ch. 8.
14. Rozzi, T. E., and G. H. In'tVeld, "Field and network analysis of interacting step discontinuities in planar dielectric waveguides," *IEEE Trans. Microwave Theory Tech*, Vol. MTT-27, 303–309, Apr. 1979.
15. Hosono, T., T. Hinata, and A. Inoue, "Numerical analysis of the discontinuities in slab dielectric waveguides," *Radio Science*, Vol. 17, 75–83, Jan.-Feb. 1982.
16. Koshiba, K., T. Miki, K. Ooishi, and M. Suzuki, "On finite element solutions of the discontinuity problem in a bounded dielectric slab waveguide," *Trans. of IECE Japan*, Vol. E66, 250–251, Apr. 1983.
17. Tsuji, M., and H. Shigesawa, "Mutual interference between the guided wave and the leaky wave regions and its effects on the performance of dielectric grating filters," *1988 IEEE/MTT-S Intern'l. Microwave Symp. Digest*, (Baltimore, MD), June 1986, pap.B-5.
18. Tsuji, M., O. Tanaka, and H. Shigesawa, "Low-loss design method of planar dielectricwaveguide y branch; Effect of serpentine taper," *IEEE Trans. Microwave Theory Tech*, Vol. MTT-39, 6–13, Jan. 1991.
19. Shigesawa, H., M. Tsuji, and O. Tanaka, "Theoretically zero-loss design of planar dielectric waveguide Y-branch: Amazing effect of serpentine-shaped taper," *1989 IEEE/MTT-S Intern'l. Microwave Symp. Digest*, (Long Beach, CA), June 1989, pap.Z-5.

20. Nasu, R., M. Tsuji, and H. Shigesawa, "A low-loss design method of dielectric Y-branch and experimental study," *The 1992 IEICE Spring Conf.*, (Noda, Japan), March 1992, C-117 (in Japanese).
21. Tanaka, O., diss. Doshisha University, March 1989 (in Japanese).
22. Tsuji, M., and H. Shigesawa, "Amazing effect of serpentine shaped taper in designing planar dielectric branch circuits," *Proc. of 20th European Microwave Conf.*, 847-852, Sept. 1990.
23. Shigesawa, H., and M. Tsuji, "Equivalent network solutions for wave scattering from finite array of conducting strips," *Proc. of URSI Intern'l Symp. on Electromagnetic Theory*, 607–609, Aug. 1989.
24. Kastner, R., and R. Mittra, "Iterative analysis of finite-sized planar frequency selective surface with rectangular patches or perforations," *IEEE Trans. Antennas Propagat.*, Vol. AP-35, 372–377, April 1987.
25. Uchida, K., T. Noda, and T. Matsunaga, "Electromagnetic wave scattering by an infinite plane metallic grating in case of oblique incidence and arbitrary polarization," *IEEE Trans. Antennas Propagat.*, Vol. AP-36, 415–422, Mar. 1988.
26. Baker, C. T. H., and E. M. Miller (Ed.), *Treatment of Integral Equations by Numerical Methods*, New York, Academic Press, 1982.
27. Walker, W. A., and C. M. Butler, "A method for computing scattering by large arrays of narrow strips," *IEEE Trans. Antennas Propagat.*, Vol. AP-32, 1327–1334, Dec. 1984.
28. Matsushima, A., and T. Itakura, "Analysis of strip gratings by singular integral equation," *Proc. Intern'l Symp. on Antennas and Propagat.*, (Tokyo, Japan), p. 261264, Aug. 1985.
29. Takenaka, T., "Scattering by a finite periodic array of strips," *1988 IEEE/AP-S Intern'l Symp. Digest*, (Syracuse, NY), 634–637, June 1988, pap. AP36-4.
30. Tsuji, M., and H. Shigesawa, *URSI/USNC National Radio Science Meeting Digest*, (Philadelphia, PA), June 1986, pap. B-15-2.
31. Tsuji, M., and H. Shigesawa, "On the electromagnetic wave scattering from planar dielectric periodic gratings with finite extent," *1987 IEEE/AP-S Intern. Microwave Symp. Digest*, (Blacksburg, VA), June 1987, pap. AP18-8.

32. Tsuji, M., and H. Shigesawa, "Wave scattering from finite metal strip gratings," *1988 IEEE/AP-S Intern. Microwave Symp. Digest*, (Syracuse, NY), June 1988, pap. AP36-3.
33. Shigesawa, H., M. Tsuji, and K. Takiyama, "Dielectric gratings as circuit components in MM and SubMM-wave regions," *Digest of 9th Intern'l Conf. on IR and MM-Waves*, (Takarazuka, Japan), Oct. 1984, pap. Th-4-6.
34. Tsuji, M., O. Tanaka, and H. Shigesawa, "Solution of the rigorous boundary-value problems of open dielectric waveguide T-branch," *Proc. of Intern'l Symp. on Antennas Propagat.*, (Tokyo, Japan), 149–152, Aug. 1989.
35. Sugahara, S., diss. Doshisha University, March 1991.
36. Shigesawa, H., M. Tsuji, and K. Takiyama, "Microwave network approach to dielectric periodic leaky wave antennas," *Proc. of Intern'l Symp. on Antennas and Propagat.*, (Kyoto, Japan), 81-84, Aug. 1985.
37. Tsuji, M., H. Shigesawa, and A. A. Oliner, "Microwave network design approach to dielectric periodic leaky-wave antennas," *1986 IEEE/AP-S Intern'l Antennas Propagat. Symp. Digest*, (Blacksburg, VA), June 1986, pap. AP05.
38. Tsuji, M., and H. Shigesawa, "An accurate analysis of discontinuities in dielectric rectangular waveguide and its application to grating filters," *1987 IEEE/MTT-S Intern'l Microwave Symp. Digest*, (Las Vegas, NV), June 1987, pap. U-4.
39. Tsuji, M., and H. Shigesawa, "Challenge to 3-D Discontinuous Dielectric Waveguide Circuit Analysis',' *1988 IEEE/MTT-S Intern'l Microwave Symp. Digest*, (New York, NY), May 1988, pap. X-5.
40. Tsuji, M., O. Tanaka, and H. Shigesawa, "A challenge of theoretically zero-loss design of 3-D dielectric waveguide Y-branch," *Proc. of Intern'l Symp. on Antennas Propagat.*, (Tokyo, Japan), l49–152, Aug. 1989.